SECOND EUROPEAN CONFERENCE ON EARTHQUAKE ENGINEERING
AND SEISMOLOGY, ISTANBUL AUG. 25-29, 2014

NUMERICAL SIMULATION OF RC FRAME TESTING WITH DAMAGED PLASTICITY MODEL. COMPARISON WITH SIMPLIFIED MODELS

Francisco LÓPEZ-ALMANSA[1], Bashar ALFARAH[2], Sergio OLLER[3]

ABSTRACT

This study aims to investigate the capacity of simplified and advanced numerical models to reproduce the nonlinear monotonic behavior of reinforced concrete framed structures. The considered simplified models are commonly used in earthquake engineering and are based either on concentrated or distributed plasticity. The considered advanced models are based on continuum mechanics and use the Damaged Plasticity Model for concrete simulation. The simplified and advanced models are used to simulate pushing experiments of a 2D RC frame. The results from the models are compared with the experiments results. That comparison shows the higher ability of the continuum mechanics models to represent the actual behavior of the frame until the collapse; the simplified models lack of the capacity to represent accurately all the phases of the behavior. This paper includes an explanation of the damage plasticity models and their implementation in the FEM package ABAQUS. A strategy to avoid the mesh sensitivity in the advanced numerical simulation of reinforced concrete structures is also described.

INTRODUCTION

The seismic structural behavior of buildings and other constructions is highly complex, involving, among other issues, complex dynamic interactions with the input ground motion, large strains and displacements, damage, plasticity and near-collapse behavior. In reinforced concrete structures, there are several structural degradation modes at the structural components level: cracking, crushing and spalling of concrete, yielding and pull-out of the tensioned reinforcement, and yielding and buckling of the compressed reinforcement.

The global seismic risk is both important and fast growing; therefore, an important research effort is being conducted worldwide to provide efficient analysis and design tools. Among them, the Incremental Dynamic Analysis (IDA) is one of the most efficient yet high costly strategies. These instruments rely on extensive testing and numerical simulation. Despite the aforementioned complexity of the seismic structural behavior, most of the numerical analyses are mainly carried out using simplified models; such models exhibit two major limitations: not all the deterioration and collapse modes are considered and the energy balance is not guaranteed. The interaction between the degradation modes is not always considered. Therefore, there is a strong need of verifying the accuracy and reliability of the obtained conclusions by comparison with more complex numerical models.

The nonlinear behavior of the RC frame is described with three types of models; they differ in the simulation of the plasticity, the consideration of the behavior of the frame elements and the type of finite elements used to discretize the structural components. Next three paragraphs explain each of the considered types of models.

[1]Professor, Technical University of Catalonia, Barcelona, francesc.lopez-almansa@upc.edu
[2]PhD Student, Technical University of Catalonia, Barcelona, bashar.alfarah@upc.edu
[3]Professor, Technical University of Catalonia, Barcelona, sergio.oller@upc.edu

Lumped plasticity models. The nonlinear behavior is concentrated in a number of zero-length plastic hinges, usually located near the connections among the frame elements. The behavior of each plastic hinge is characterized by force-displacement laws is considered by means of interaction surfaces. These models have been implemented in the most widely used software in earthquake engineering SAP-2000 v.16 (Computers & Structures 2012) using the general frame formulation (Bathe, Wilson 1976). The hinge properties are obtained according to Tables 6-7 and 6-8 of (FEMA 356 2000).

Distributed plasticity models. Fiber section models are used to simulate the spread of plasticity along the member length and across the section. Each fiber is associated with a uniaxial stress strain relationship, and then the sectional behavior is obtained by integration imposing the Navier-Bernouilli hypothesis. The distributed plasticity models can be implemented with the classical displacement-based finite elements formulations (Hellesland, Scordelis 1981; Marí, Scordelis 1984), or with the more recent force-based formulations (Spacone et al. 1996; Neuenhofer, Filippou 1997). In a displacement-based approach, the displacement field is imposed, whilst in a force-based formulation the equilibrium is strictly satisfied and no restraints are imposed to the development of inelastic deformations throughout the member; in this research, we use a software code (Seismosoft 2013) that considers both formulations. A uniaxial constant-confinement model (Mander et al.1988; Martínez-Rueda, Elnashai 1997) describes the concrete behavior. The steel behavior is represented by the Monti-Nuti uniaxial model (Menegotto, Pinto 1973) with isotropic hardening (Filippou et al. 1983); this model is able to describe the post-elastic buckling behavior of reinforcing bars under compression (Monti et al. 1996).

Continuum mechanics-based models. The concrete frame members are discretized with 3D 8-node hexahedron solid finite elements and the reinforcement bars are represented by 2-node truss elements. The concrete behavior is represented by multiaxial damaged plasticity model (Lubliner et. al.1989) with the modifications of the yield surface proposed by (Lee and Fenves 1998). A normal plasticity model is used to simulate the nonlinear monotonic behavior of steel. The joint behavior of concrete and steel is described by the "embedded element technique". The relationship between the accuracy of the results and the size of the mesh (mesh sensitivity) is assessed. The time integration is carried out following mainly an implicit formulation. The global model is generated by imposing the energy balance. The analysis is carried out for large displacements but not for large strains. Such models are implemented in the ABAQUS code (ABAQUS 2013; López Almansa et al. 2012; Castro et al. 2014).

SIMULATED EXPERIMENT

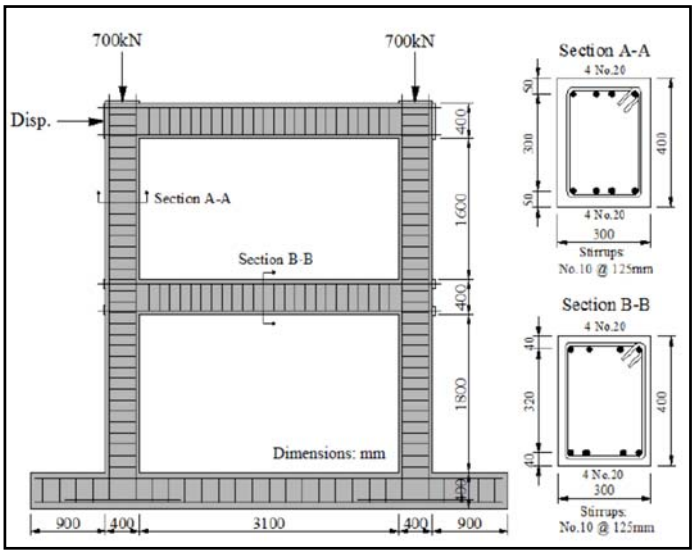

Figure 1. Tested frame (Vecchio, Emara1992)

These models have been used to simulate the static tests described in (Vecchio and Emara 1992); the experiment consisted of pushing a laboratory single-bay two-story RC plan frame. Figure 1 shows the geometric properties of the tested frame as well the reinforcement details (Vecchio, Emara 1992) for more details. Material properties were determined from concrete cylinder tests and steel coupon tests,

as summarized in Table 1. The frame had been previously simulated by some of the authors (Faleiro et al. 2005; Faleiro et al. 2008; Güner 2008).

Reinforcement Bars									Concrete
Bar No.	A_s (mm^2)	D_b (mm)	f_y (MPa)	f_u (MPa)	E_s (GPa)	E_{sh} (MPa)	ε_{sh}	ε_u	f'_c (MPa)
No. 20	300	19.5	418	596	192.5	3100	0.0095	0.0669	30
No. 10	100	11.3	454	640	200	3100	0.0095	0.0695	

Table 1. Material Properties (Güner 2008)

NUMERICAL SIMULATION OF THE EXPERIMENT

Lumped plasticity models

In this model a nonlinear spring "hinge" element has been assigned at each end of each componenet (beam and column). The nonlinear behavior of these hinges is governed by a backbone curve, represents the full behavior of the expected reinforced concrete hinges. For this modeling a FEM backage from Computers and Structures Inc has been used SAP2000 to simulate the exeperimental RC frame. Based on this backbone curve as shown in Figure 2 no plastic deformation occurs until point B where the hinge yields. This is followed by a yield plateau or strain hardening behavior until point C which represents the ultimate capacity of the hinge. After point C, the hinge's force capacity immediately drops to point D which corresponds to the residual strength of the hinge. Point E represents the ultimate displacement capacity of the hinge after which total failure of the hinge is reached at point F (Computers & Structures 2012). There are three stages marked between point B and C for information purposes:IO corresponds to immediate occupancy, LS to life safety, and CP to collapse prevention. A moment rotation hinges have been assigned to the beams and interacting P-M plastic hinges have been assigned to the columns elements. All joints have been assumed as a rigid joints with zero hinge length located at the face of the joints. The hinge properties are obtained according to Tables 6-7 and 6-8 of (FEMA 356 2000) based on the material properties, element's cross section and reinforcement details. The most critical part in the nonlinear modeling process with SAP2000 is the hinge locations and the selected hinge properties they have a great influence on the computed response. In addition to the moment and P-M hinges, a shear hinge could be assigned to the model but these shear hinges do not interact with the other hinges. In other words, the lumped plastic hinges work individually without any interaction, for example, in case a shear hinge had developed in a column the shear degradation has no influence on the axial capacity of the column.

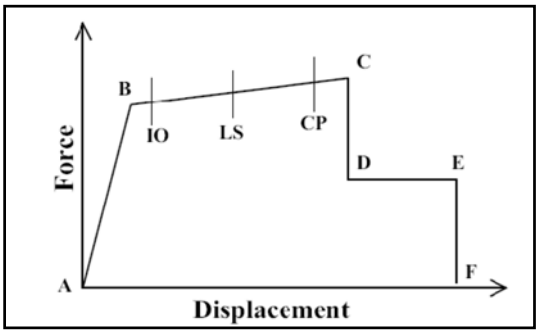

Figure 2. Hinge behavior (FEMA 356 2000)

Distributed plasticity models

Two models have been derived using the fiber element model to represent the nonlinear behavior of the tested frame. The first model adopts the force-based formulation by using one finite element for each component, we will symbolize for this model in this paper by FB element model. Second model adopts the displacement-based formulation by using five finite elements for each component and will symbolize for this model by DB element model. The FEM package SeismoStruct V6.5 has been used to simulate

the experiment by using the (Mander et al. 1988) nonlinear concrete model using a confinement factor to distinguish between the confinement (core) and un-confinement concrete (cover) material. Monti-Nuti steel model has been used to model the behavior of the reinforcing bars taking into account the post-elastic buckling behavior under compression. The cross section for each element is divided into 250 fibers in order to achieve more accuracy; five integration points have been used along the length of each element. Figure 3 shows the fiber element model and the integration points "Gauss point" along the element. The accuracy of the solution can be improved for the FB elements by either increasing the number of Gauss points or the number of the elements; for DB elements, this can be done only by increasing the number of elements. The main limitation of this model is the ability to consider just the flexural effects, in another word the accurate simulation of reinforced concrete members dominated by shear or the interaction between the shear and flexure and axial capacity cannot be achieved through this model. Figure 3 shows an example of the distributed plasticity model that is used in this study.

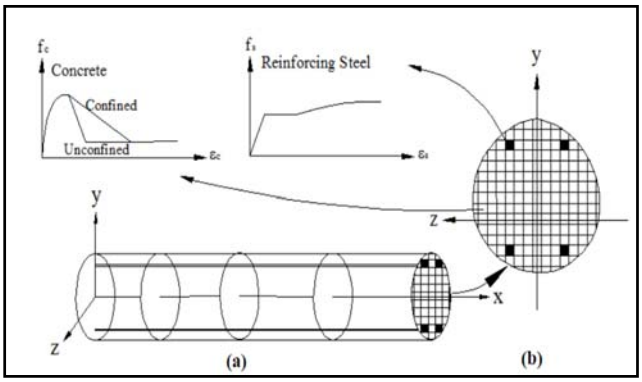

Figure 3. Fibre Element: (a) Distribution of control sections; (b) Section subdivision into fibres (Taucer et al. 1991)

Continuum mechanics-based models

The main concepts of continuum mechanics are implemented to simulate the complicated nonlinear behavior of the reinforced concrete material in order to evaluate the behavior of reinforced concrete structures. It is essential to be able to predict their response under any type and level of loading and must take into account all aspects of the nonlinear behavior of RC and especially for high loads levels, such as earthquakes. Numerical modeling should take into account these effects to produce realistic predictions of strength, stiffness and seismic energy dissipation capacity. For this objective, the 3D solid finite element are used to simulate the concrete material and 3D truss element for the reinforcing bars. The main advantage of employing a computationally more expensive three-dimensional 3D solid finite element for RC analysis is that it can take into account any triaxial stress state developed in almost all types of RC structures as well as all the failure modes (e.g., brittle shear failure, crushing and cracking) by considering the interaction between all the degradation modes (e.g., concrete spalling and the effects on the rebar buckling, the interaction between the shear capacity and the axial capacity of the element etc.) that are not easily predicted by simpler models. In such an analysis, there are three aspects that need to be considered: (a) modeling of concrete, (b) the material model to describe the behavior at the interface and (c) modeling of reinforcement within the concrete mesh (G. C. Lykidis1 et al. 2008). And because of the properties of the concrete material and the relation between concrete and steel material the simulation of RC structures pose a challenge, concrete has different behavior and different degradation modes it's much quicker undergoes degradation under tension than compression. The interaction between the reinforcing bars and the surrounding concrete has a significant impact on the overall response of the structures and especially under the cyclic loads, the degradation of material in each element of the structure can influences on the overall behavior of the whole structure and can participates in performing several collapse mechanism. All of this poses difficulties for numerical analyses. The selected constitutive models of materials and the parameters of these models needed to be correctly selected. In this simulation the advanced FEM software ABAQUS has been used to simulate the tested frame. The Concrete Damaged Plasticity Model (CDPM) has been used to simulate the

concrete material by using C3D8R Brick element. Normal plasticity model has been used for the steel material by using a T3D2 truss element. Embedded element technique adopted to represent the relation between both materials. Where the reinforcing bars elements "the guest" are embedded in the concrete elements "the host". The translational degrees of freedom at the node of the guest elements are eliminated and the node becomes an "embedded node". The translational degrees of freedom of the embedded node are constrained to the interpolated values of the corresponding degrees of freedom of the host element (ABAQUS 2013). The element mesh size is 5 cm.

As mentioned before, the parameters of the used constitutive models have the biggest effects on the obtained performance, and in order to obtain the most accurate results we will describe in the following paragraphs the parameters of CDPM and the way to obtain these parameters and how to avoid the mesh sensitivity.

CONCRETE DAMAGED PLASTICITY MODEL (CDPM)

General description

It is assumed that the main two concrete failure mechanisms are the tensile cracking and compression crushing of the concrete material. This model could be considered as one of the best models to represent the complex behavior of concrete material by using the concepts of isotropic damaged elasticity in combination with isotropic tensile and compressive plasticity to represent the inelastic behavior of concrete, this model has been designed for applications in which concrete is subjected to monotonic, cyclic and/or dynamic loading, and consists of the combination of non-associated multi-hardening plasticity and scalar (isotropic) damaged elasticity to describe the irreversible damage that occurs during the fracturing process. This model was developed by (Lubliner et al. 1989) and elaborated by (Lee & Fenves 1998). This model has been implemented in the FEM code (ABAQUS, 2013) under the name *CONCRETE DAMAGED PLASTICITY MODEL (CDPM)*. This model assumes non-associated potential plastic flow. The flow potential *G* used for this model is the Drucker-Prager hyperbolic function:

$$G = \sqrt{(\epsilon \sigma_{t0} \tan\psi)^2 + \bar{q}^2} - \bar{p}\tan\psi \tag{1}$$

σ_{t0} is the uniaxial tensile stress at failure, $\bar{p}$ is the hydrostatic pressure stress, $\bar{q}$ is the Mises-equivalent effective stress, ψ is the *dilatancy* angle measured in the *p-q* plane at high confining pressure, and ϵ is an eccentricity of the plastic potential surface. The plastic-damage concrete model uses a yield condition based on the loading function *F* proposed by (Lubliner et al. 1989) with the modifications proposed by (Lee, Fenves 1998) to account for different evolution of strength under tension and compression in the form:

$$F = \frac{1}{1-\alpha}\left(\bar{q} - 3\alpha\,\bar{P} + \beta(\tilde{\varepsilon}^{pl})\,\langle \sigma_{max} \rangle - \gamma\langle -\sigma_{max} \rangle\right) - \overline{\sigma_c}\,\tilde{\varepsilon}_c^{pl} = 0 \tag{2}$$

$$\alpha = \frac{(\sigma_{b0}/\sigma_{c0}) - 1}{2(\sigma_{b0}/\sigma_{c0}) - 1}\ ; 0 \le \alpha \le 0.5;\ \beta = \frac{\overline{\sigma_c}(\tilde{\varepsilon}_c^{pl})}{\overline{\sigma_t}(\tilde{\varepsilon}_t^{pl})}(1-\alpha) - (1+\alpha);\ \gamma = \frac{3(1-K_c)}{2K_c - 1} \tag{3}$$

Parameter α depends on the ratio of the biaxial and uniaxial compressive strengths (σ_{b0}/σ_{c0}), K_c is the ratio of the second stress invariant on the tensile meridian to that on the compressive meridian it must satisfy the condition $0.5 < K_c \le 1.0$. It is clearly seen, that the behavior of concrete depends on four constitutive parameters (K_c, ψ, σ_{b0}/σ_{c0}, ϵ). Other parameters such as tensile uniaxial strength and uniaxial or biaxial compressive strength of concrete should be taken from testing. Since concrete exhibits softening behavior and stiffness degradation that often lead to severe convergence difficulties, in implicit analysis a visco-plastic regularization technique has been added to the *CDPM* to permit stresses to be outside of the yield surface by using a viscosity parameter μ (ABAQUS 2013).

Dilatancy angle (ψ)

Dilation in a frictional material is the phenomenon of change of the inelastic volume due to plastic deviation as shown in Figure 4. For concrete is ψ =13° (Vermeer, de Borst 1984)

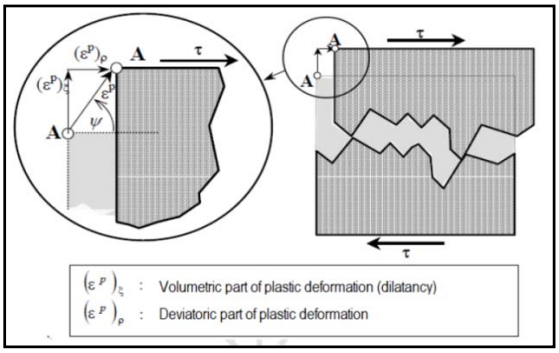

Figure 4. Dilatancy angle (Oller 2013)

As mentioned before, K_c is the ratio of the second stress invariant on the tensile meridian to that on the compressive meridian or in another word the ratio between the magnitude of the deviatory stress in uniaxial tension to uniaxial compression. To obtain the value of K_c we will use the Mohr-Coulomb yield surface function as given in equation (4) to calculate the value of K_c

$$F(\rho,\zeta,\theta,\phi,c) = \sqrt{2}\,\zeta \sin\phi + \sqrt{3}\,\rho \sin\left(\theta+\frac{\pi}{3}\right) + \rho\cos\left(\theta+\frac{\pi}{3}\right)\sin\phi - \sqrt{6}\,c\cos\phi = 0 \qquad (4)$$

At π plan ζ = 0 and for θ + π /6 "tension meridian plan" we can calculate the magnitude of the deviatory stress in uniaxial tension at yield (ρ_{t0}). The magnitude for uniaxial compression (ρ_{c0}) could be calculated for θ = – π /6 as given in equation (5):

$$\rho_{t0} = \frac{2c\sqrt{6}\cos\phi}{3+\sin\phi}, \rho_{c0} = \frac{2c\sqrt{6}\cos\phi}{3-\sin\phi} \qquad (5)$$

For ϕ = 32° the friction angle of concrete we can obtain the value of K_c.

$$K_c = \frac{\rho_{t0}}{\rho_{c0}} = \frac{3-\sin\phi}{3+\sin\phi} = 0.7 \qquad (6)$$

Figure 5 represents the yield surface in the deviatory plan for several values of K_c.

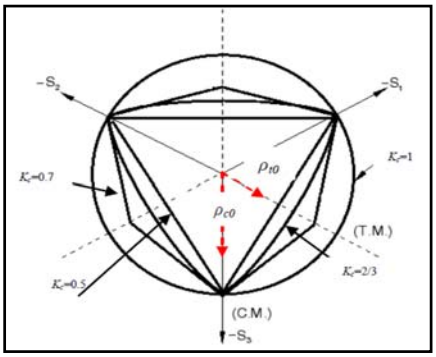

Figure 5. Yield surface in the deviatory plan for several values of K_c

CDPM's parameters that have been used in this study are summarized in Table 2.

CDPM Parameters				
K_c	ψ	σ_{b0}/σ_{c0}	ϵ	μ
0.7	13	1.16	0.1	0

Table 2. CDPM's parameters.

Uniaxial compression behavior

The stress-strain behavior under sustained compressive loading is modeled in three phases as shown in Figure 6(a).

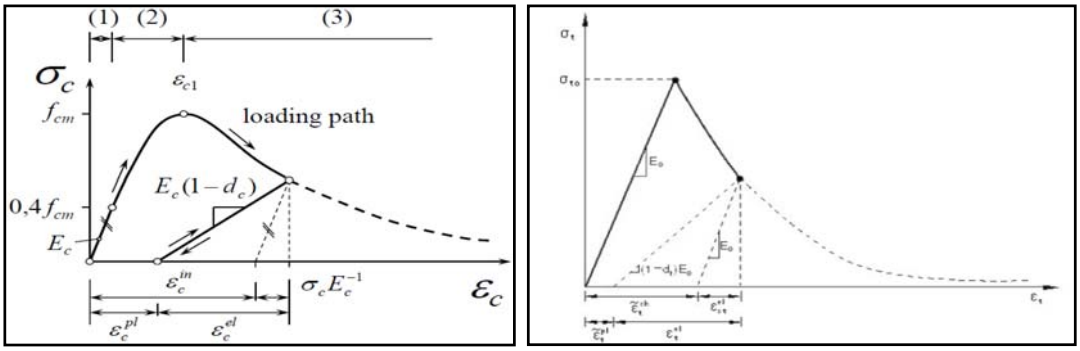

(a) Compression (Birtel, Mark 2006) (b) Tension (Abaqus 2013)

Figure 6. Uniaxial model of the concrete behavior

The first two phases describe the ascending branch up to the peak load f_{cm} at ε_{c1}. Their formulations are similar to the recommendations of the Model Code (CEB-FIB 1993). The third and descending branch takes account for its dependency on the specimen geometry (Vonk 1993; Van Mier 1984) to ensure almost mesh independent simulation results. Thus, $\sigma_{c(3)}$ incorporates within the descent function γ_c the constant crushing energy G_{cl} (Krätzig & Pölling, 2004) and the finite element size l_{eq}.

First phase:

$$\sigma_{c(1)} = E_c\ \varepsilon_c \tag{7}$$

Second phase:

$$\sigma_{c(2)} = \frac{E_{ci}\ \frac{\varepsilon_c}{f_{cm}} - (\varepsilon_c/\varepsilon_{c1})^2}{1 + \left(E_{ci}\ \frac{\varepsilon_{c1}}{f_{cm}} - 2\right)\frac{\varepsilon_c}{\varepsilon_{c1}}} f_{cm} \tag{8}$$

Third phase:

$$\sigma_{c(3)} = \left(\frac{2 + \gamma_c f_{cm}\ \varepsilon_{c1}}{2 f_{cm}} - \gamma_c\ \varepsilon_c + \frac{\varepsilon_c^2\ \gamma_c}{2\varepsilon_{c1}}\right)^{-1} \tag{9}$$

$$\gamma_c = \frac{\pi^2 f_{cm}\ \varepsilon_c}{2\left[\frac{G_{cl}}{l_{eq}} - 0.5 f_{cm}\left(\varepsilon_c\ (1-b) + b\,\frac{f_{cm}}{E_c}\right)\right]^2}, b = \frac{\varepsilon_c^{pl}}{\varepsilon_c^{in}} \tag{10}$$

E_{ci} is the modulus of elasticity (MPa) at a concrete age of 28 days; f_{ck} is the characteristic strength (MPa) at a concrete age of 28 days. $f_{cm} = f_{ck} + \Delta f$, Δf = 8 MPa, f_{cm0} = 10 MPa, ε_{c1} = 0.0022.

$$E_{ci} = E_{c0}\ [f_{cm}/f_{cm0}]^{1/3} \tag{11}$$

$$E_c = 0.85 E_{ci} \tag{12}$$

Uniaxial tension behavior

The stress-strain relation for tensile loading consists of a linear part up the strength σ_{t0} and a nonlinearly descending part as shown in Figure 6 (b). The softening function is derived from the stress-crack opening relation (Hordijk 1992) and it is related directly to the finite element mesh size.

$$\sigma_{t0} = f_{ctk0,m}\left(\frac{f_{ck}}{f_{ck0}}\right)^{2/3} \tag{13}$$

$f_{\mathrm{ctk0,m}} = 1.4$ MPa and $f_{\mathrm{ck0}} = 10$ MPa (CEB-FIB 1993). The relation between the maximum tensile strength and the tensile stress for any value of the crack width (w) between zero and w_c could be calculated from the following equation (for $c_1 = 3$, $c_2 = 6.93$):

$$\frac{\sigma_{t(w)}}{\sigma_{t0}} = [1 + (c_1 w/w_c)^3]e^{-c_2 \frac{w}{w_c}} - \frac{w}{w_c}(1 + c_1^3)e^{-c_2} \quad (14)$$

w_c is the critical crack opening that needs the energy G_F to develop, could be calculated according to (Hordijk 1992)

$$w_c = 5.14\, G_F / \sigma_{t0} \quad (15)$$

G_F is the "fracture energy of concrete" which is required energy to propagate a tensile crack of unit area, could be calculated according to (CEB-FIB 1993) by the following equation:

$$G_F = G_{F0}\,(f_{cm}/f_{cm0})^{0.7} \quad (16)$$

G_{F0} is the base value of fracture energy; it depends on the maximum aggregate size d_{max}, (Table 2.13- CEB-FIB 1993). To draw the tensile stress strain curve after the maximum strength, the values of the tensile strain take from the following equation:

$$\varepsilon_t = \varepsilon_{t0} + w/l_{eq} \quad (17)$$

An exponential function has been used to calculate do damage variable for both of compression and tension

$$d_c = 1 - \exp^{(-a_c\ \varepsilon_c^{in})} \quad (18)$$

$$d_t = 1 - \exp^{(-a_t\ \varepsilon_t^{ck})} \quad (19)$$

a_t and a_c are model parameters for uniaxial tension and compression respectively, and can be calibrated from the uniaxial tensile and compressive tests by imposing the conditions:

$$\varepsilon_c^{pl} = 0 \Rightarrow d_c = 0\ \&\ \varepsilon_c^{pl} = \varepsilon_{c\,max}^{pl} \Rightarrow d_c = 1 \quad (20)$$

$$\varepsilon_c^{pl} = 0 \Rightarrow d_c = 0\ \&\ \varepsilon_c^{pl} = \varepsilon_{c\,max}^{pl} \Rightarrow d_c = 1 \quad (21)$$

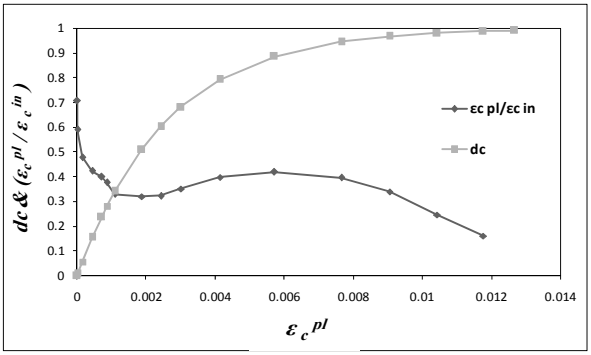

Figure 7. Compression damage vs. compressive plastic strain. Ratio of the compressive plastic strain to the crushing strain vs. compressive plastic strain ($ac = 2800$)

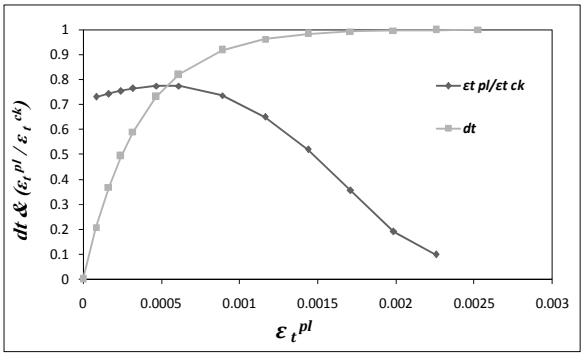

Figure 8. Tension damage vs. tensile plastic strain. Ratio of tensile plastic strain to the cracking strain vs. tensile plastic strain ($a_t = 380$)

Since the values of a_c and a_t are imposed and in order to avoid any negative values during the analysis for both of compressive and tensile plastic strain (ε_c^{pl}, ε_t^{pl}) and to ensure a decreasing or at least to avoid the increasing in the ratio of the compressive plastic strain to the crushing strain ($\varepsilon_c^{pl} / \varepsilon_c^{in}$) and the tensile plastic strain to the cracking strain ($\varepsilon_t^{pl} / \varepsilon_t^{ck}$) it is better to plot the both curves together

(damage versus plastic strain and the strains ratio versus the plastic strain), this plot gives the impression of the damage evolution and the effect of this evolution on the plastic strains, since the ratio of the plastic strain to the crushing/cracking strain should decreases in conjunction of increasing the plastic strain as shown in Figures 7 and 8.

Table 3 summarizes the needed values to build the input compressive / tensile behavior data in CDPM (ABAQUS 2013).

f_{ck} (MPa)	d_{max} (mm)	G_{F0} N/mm	G_F N/mm	a_c	a_t	G_{cl} N/mm	l_{eq} (mm)	b
30	16	0.03	0.0763	2800	380	10	50	0.35

Table 3. Concrete material parameters

NUMERICAL RESULTS

Figure 9 shows the comparison of experimental and analytical results for the examined frame. It can be observed that the lumped plasticity model with just flexural or P-M interaction plastic hinges has failed to predict the overall response of the frame, the maximum lateral force capacity of this model didn't match with the real value with difference (–10%), the structure in this model had collapsed at lateral displacement almost (–50%) of the ultimate displacement of the experiment. In the other hand the distributed plasticity models showed a better performance in general. DB element model over predicts the frame capacity with difference (+8.7%), FB predicts the lateral capacity with difference (–3%), both model succeed to avoid the earlier collapse and resist more displacement than the lumped model. Distributed plasticity models couldn't capture very well the overall behavior especially after development of the first cracks in beams and columns "the softening stage between the initial stiffness and the ultimate capacity". Further investigation has been carried out on the performance of distributed plasticity models. As shown in Figure 10, the significant effect of including the geometric nonlinearity in the analysis. Without including the P-delta effect the structure remains able to resist more lateral force without any softening which is not fitting with the real behavior. In case of considering P-delta in the analysis the structure starts to show the softening after reaching the ultimate value directly without demonstrate any ductility. We can conclude that the main reason of the softening in these distributed plasticity models is the geometric nonlinearity. Whilst in the real behavior this geometric nonlinearity has a influence on the capacity of the structure, accounting at about 12% of the total overturning moment acting on the structure at ultimate (Vecchio, Emara 1992). Moreover, the experimental frame had demonstrated a very good ductility after achieving the ultimate load before degrading the lateral capacity.

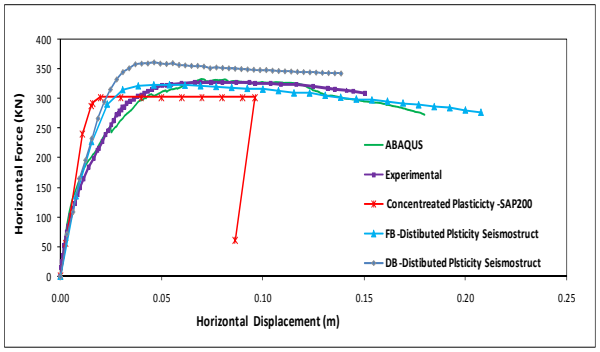

Figure 9. Experimental and simulated capacity curves

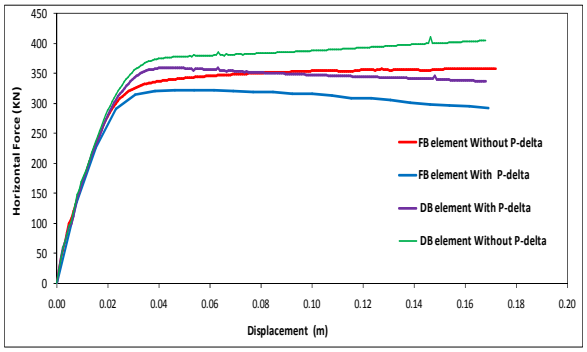

Figure 10. Capacity curves based on distributed plasticity models with and without considering geometric nonlinearity

The continuum mechanics model with CDPM observed a superiority to predict the overall behavior of the frame during the experiment. This model reached the ultimate capacity with difference (0.3%) comparing with the experimental one, all phases have been predicted very well by this model "initial stiffness, softening after the first cracks, ultimate force, ductility phase and collapse phase". First

crack has been developed in the beam of the first floor (Vecchio, Emara 1992). This model succeed to predict this crack as shown in Figure 11. Tensile damage during the experiment and until displacement (18 cm) is shown in Figures 12, 13 and 14.

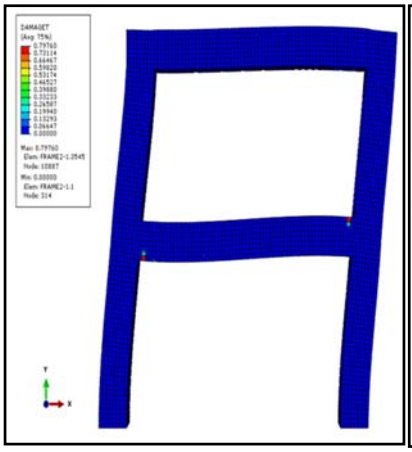

Figure 11. First crack in the first story's beam

Figure 12. Tension damage (at lateral displacement 7 mm)

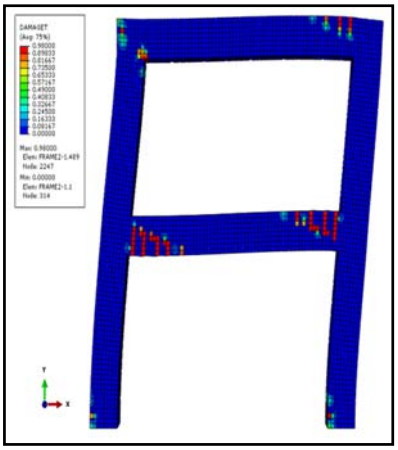

Figure 13.Tension damage (at lateral displacement 1 cm)

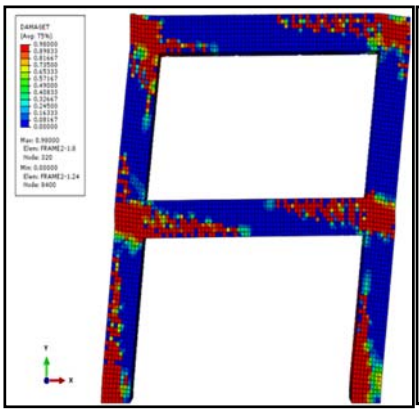

Figure 14. Tension damage at last state

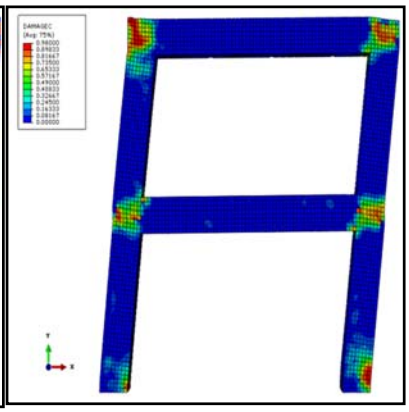

Figure 15. Compression damage at last state

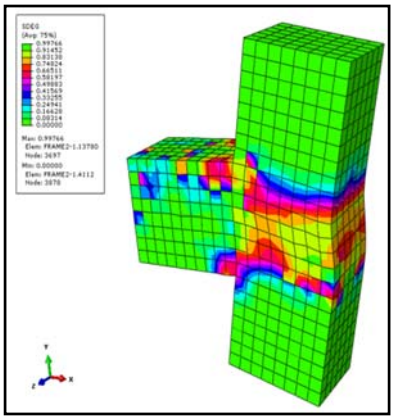

Figure 16. Damage in the north joint in the first story at last state

Continuum mechanics model succeed to predict the crushing “compression damage” at the last displacement as well the yielding in the reinforcing bars in columns and beams, the damage in the joint also has predicted very well as shown in Figures 15, 16 and 17.

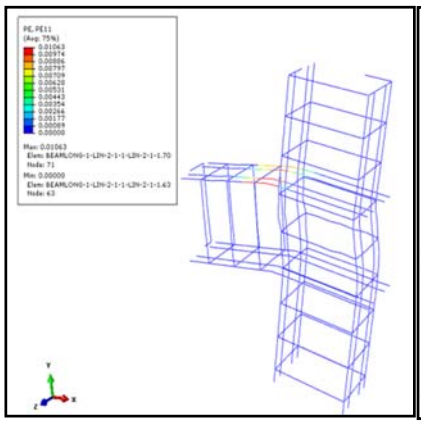

Figure 17. Yielding of reinforcing bars at first story's north joint at last state

Figure 18. Last Condition of the base joint of the South Column

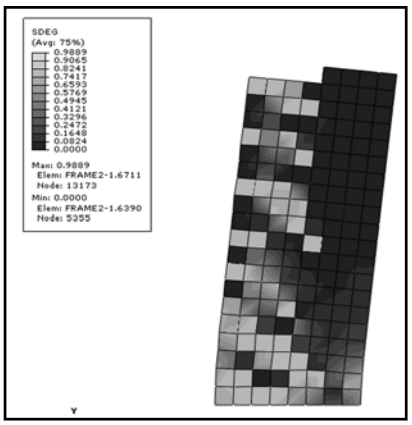

Figure 19. Last Damage in the base joint of south column

The damage at last drift (2%) matched very well with the last condition of the base joint of the south column as shown in Figures 18 and 19. Table 4 shows a comparison between the experimental results and the obtained one using several models.

	SAP2000	SeismoStruct FB	SeismoStruct DB	ABAQUS	Experiment
Ultimate Force (KN)	302	322	361	333	332
First Plastic Hinge Developed at	Beam 1st Story	Beam 1st Story	Beam 1st Story	Beam 1st Story	Beam 1st Story
Failure Mechanism	6 Plastic Hinges	6 Plastic Hinges	6 Plastic Hinges	6 Plastic Hinges	6 Plastic Hinges
Joints Damage	N/A	N/A	N/A	YES	YES
Force at First Crack in Beam First Story	N/A	N/A	N/A	61	52.5
Force at First Crack in the column at the base	N/A	N/A	N/A	135	145
Force at first yielding in the column's reinforcement	N/A	295	327	305	323

N/A: Not Available

Table 4. Comparison of Numerical and Experimental Results of The Tested Frame.

CONCLUSIONS

A numerical modeling of a full scale experimental RC frame subjected to monotonic loading has been carried out by using several FE models and several constructive material models. The obtained results showed the inability of the simplified models to predict the real behavior of the RC frame correctly. Lumped plasticity models failed to reach the ultimate lateral force capacity as well to reach the maximum lateral displacement. Lumped plasticity model has succeeded to predict the locations of plastic hinges in both of columns and beams. Distributed plasticity models have succeeded to exceed the earlier collapse and go further in resisting the applied displacement more than the lumped models. Distributed plasticity model with FB formulations showed better performance than DB formulation models in reaching the ultimate force and matching in general the real performance. Both Distributed plasticity models showed stiffer behavior and inability to represent correctly the ductility and softening of the frame. They failed as well to reach the correct maximum lateral force capacity. Moreover the main reason of the degradation directly after achieving the maximum lateral force capacity in the distributed plasticity models is the geometric nonlinearity which had a significant effect on the real frame but after a very good state of ductility. Continuum mechanics-based model using CDPM showed a superior ability to reproduce the real performance of the experimental RC frame. Embedded element technique demonstrated a very good performance as a tool to simplify the modeling of the relation between concrete and rebar under monotonic loading and even after achieving several degradation states (e.g., cracking and crushing etc.). A great attention should be paid to the value of CDPM's parameters as well the compression / tension stress strain input data by taking into account the FE's mesh size.

REFERENCES

ABAQUS analysis user's manual version 6.11.3. (2013). Pawtucket (RI): Hibbitt, Karlsson & Sorensen.

Bathe KJ, Wilson EL (1976). Numerical Methods in Finite Element Analysis, *Prentice-Hall*.

Birtel V, Mark P (2006). Parametrised Finite Element Modelling of RC Beam Shear Failure. Abaqus Users Conference.

Castro JC, López Almansa F, Oller S (2014). Modelización numérica del comportamiento estructural cíclico de barras esbeltas de acero con pandeo restringido, RIMNI. Pending.

CEB-FIP (1993). Model Code 1990. Thomas Telford, London.

Computers & Structures Inc. (2012). CSI Analysis Reference Manual for SAP2000®, ETABS®, and SAFE™, available from www.comp-engineering.com.

Faleiro J, Barbat A, Oller S (2005). Plastic damage model for nonlinear reinforced concrete frames analysis, *VIII International Conference on Computational Plasticity (COMPLAS VIII), CIMNE.*

Faleiro J, Oller S, Barbat A (2008). Plastic-damage analysis of reinforced concrete frames, *Engineering* Computations, 27(1):57-83.

FEMA 356 (2000). Prestandard and commentary for the seismic rehabilitation of buildings, *Federal Emergency management Agency.*

Filippou FC, Popov EP, Bertero VV (1983). Effects of bond deterioration on hysteretic behavior of reinforced concrete joints, Report EERC: 83-19, University of California, Berkeley.

Hellesland J, Scordelis A (1981). Analysis of RC bridge columns under imposed deformations, IABSE Colloquium, *Delft* 545-559.

Hordijk, DA (1992). Tensile and tensile fatigue behavior of concrete; experiments, modeling and analyses, *Heron* 37(1):3-79.

Krätzig, WB, Pölling R (2004). An elasto-plastic damage model for reinforced concrete with minimum number of material parameters, *Computer and Structures* 82(15-16): 1201-1215.

Lee J, Fenves GL (1998). Plastic-Damage Model for Cyclic Loading of Concrete Structures, *Engineering Mechanics* 124(8):892–900.

López-Almansa F, Castro JC, Oller S (2012). A numerical model of the structural behavior of buckling-restrained braces, *Engineering Structures*, 41(1):108–117.

Lubliner J, Oliver J, Oller S, Oñate E (1989). A plastic-damage model for concrete, *Solids and Structures*, 25(3):299–326.

Mander JB, Priestley MJN, Park R (1988). Theoretical stress-strain model for confined concrete, *of Structural Engineering*, 114(8):1804-1826.

Marí A, Scordelis A (1984). Nonlinear geometric material and time dependent analysis of three dimensional reinforced and prestressed concrete frames, Report 82-12, University of California, Berkeley.

Martínez-Rueda JE, Elnashai AS (1997). Confined concrete model under cyclic load, *Materials and Structures*, 30 (3):139-147.

Menegotto M, Pinto PE (1973). Method of analysis for cyclically loaded RC plane frames including changes in geometry and non-elastic behavior of elements under combined normal force and bending, *IABSE Colloquium*, Zurich 15-22.

Monti G, Nuti C, Santini S (1996). CYRUS. Cyclic Response of Upgraded Sections, Report No. 96-2, University of Chieti, Italy.

Neuenhofer A, Filippou FC (1997). Evaluation of nonlinear frame finite-element models, *Structural Engineering*, 123(7): 958-966.

Güner S (2008). Performance assessment of shear-critical reinforced concrete plane frames, PhD. Thesis, University of Toronto.

Oller S (2013). Nonlinear Dynamics, International Center For Numerical Method in Engineering, Technical University of Catalonia.

Seismosoft (2013). SeismoStruct v6.5 – A computer program for static and dynamic nonlinear analysis of framed structures, available from http://www.seismosoft.com.

Spacone E, Ciampi V, Filippou FC (1996). Mixed formulation of nonlinear beam finite element, *Computers & Structures*, 58(1):71-83.

Taucer F, Spacone E, Filippou FC (1991). A Fiber Beam-Column Element for Seismic Response Analysis of Reinforced Concrete Structures, University of California, Berkeley, Report No. 91/17.

Van Mier, JGM (1984). Strain-softening of concrete under multiaxial loading conditions PhD Thesis, Technical University of Eindhoven.

Vecchio F, Emara MB (1992). Shear Deformations in reinforced Concrete Frames, *ACI Structural Journal*, 89(1):46-56.

Vermeer PA, de Borst R (1984). Non-associated plasticity for soils, concrete and rock, *Heron* 29(3):3–64.

Vonk RA (1993). A micromechanical investigation of softening of concrete loaded in compression, *Heron* 38 (3):3-94.